Pathloss Models for Indoor Hotspot Deployment at 83.5 GHz

Camillo Gentile†, Jelena Senic‡, Peter B. Papazian‡, Jae-Kark Choi†, and Kate A. Remley‡
National Institute of Standards and Technology
Communications Technology Laboratory
Wireless Networks Division† Radio-Frequency Technology Division‡
Gaithersburg, Maryland, USA Boulder, Colorado, USA

***Abstract* — Conventional pathloss models are based on the received power from an omnidirectional antenna. Millimeter-wave receivers, conversely, will feature highly directional antennas that can be steered towards the angle with maximum power, exploiting their high gain in order to compensate for the greater pathloss witnessed in the upper spectrum. Hence models for the maximum power are also valuable. In this paper, we present both model types for indoor hotspot deployment at 83.5 GHz. The environments considered – a basement, lobby, and hallway in line- and non-line-of-sight conditions up to 24 m range – are typical of such deployments. To fit the models, a measurement campaign with over 1500 different transmitter-receiver configurations was conducted using a correlation-based channel sounder. Computation of the maximum-power model is enabled by the sounder's custom-designed antenna array which can resolve the receiver power into three-dimensional angles-of-arrival.**

Keywords — E band; mmWave; millimeter-wave; channel propagation modeling; wireless system

Figure 1: Custom-designed 16-port octagonal receiver antenna array.

I. Introduction

Over less than a decade, radio-frequency transmission from data-intensive mobile devices has created a "spectrum crunch" below 6 GHz, prompting the wireless community to investigate the millimeter-wave band (30 – 300 GHz) as an alternative [1]. Although propagation is less favorable in this regime, channels with much wider bandwidths will be available. To effectively design communication systems here, fundamental understanding of the propagation characteristics expressed through channel models is required. The most basic and useful of models for link-layer analysis is pathloss. To our knowledge, indoor pathloss models for next-generation Wireless Local Area Networks (WLAN) and Local Multipoint Distribution System (LMDS) deployments are still lacking to date.

The choice spectrum allocated by the Federal Communications Commission (FCC) for fixed-mobile, up to 850 MHz wide, lies on the band edge around 30 GHz [2]. Hence a reasonable number of publications for indoor pathloss models there have already appeared in the literature. Some of the most recent, which consider obstructed- and/or non-line-of-sight in the range up to tens of meters, are [3][4][5]. Similar set-ups can be found at 60 GHz in [6][7][8]: although less favorable due to oxygen absorption loss, it is still attractive given the broad unlicensed band from 57-63 GHz (recently extended as 57-71 GHz). As such, these two bands have been studied the most.

The E band (71-76 GHz, 81-86 GHz, and 92-95 GHz) has received significantly less attention than 60 GHz due to licensing requirements and greater freespace propagation loss. Nevertheless, the fact that it is not subject to oxygen absorption loss more than compensates for the latter; hence the lack of propagation measurements, both indoors and outdoors, for this band is surprising: in [9], spatio-temporal models are provided at 72 GHz (and 63 GHz) for an office environment from 24 measurements, however only in line-of-sight (LOS) conditions up to a range of 10 m. In [10], wideband measurements were taken at 70, 88, and 108 GHz in LOS up to 6 m. Less recently, slightly longer-range measurements were taken at 94 GHz in LOS and obstructed-LOS conditions [11][12]. And in [13], pathloss models and dispersion statistics in LOS and non-LOS (NLOS) at 73 GHz (and 28 GHz) are provided for an indoor office environment; the models were collected for 48 different TX-RX configurations in the range 4 - 46 m.

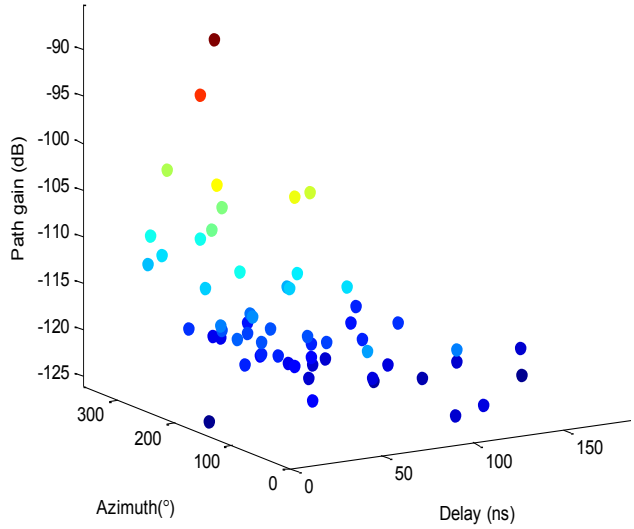

Figure 2: Directional channel impulse response of an example TX-RX configuration. Each circle indicates an extracted multipath-channel component color-coded according to path gain.

In this paper, we present pathloss models at 83.5 GHz for two indoor environments: a basement and a lobby / hallway area. The models were generated from measurements over 1500 different transmitter-receiver configurations using a correlation-based channel sounder. Conventional pathloss models are based on received power from an omnidirectional antenna. Millimeter-wave receivers, however, are envisioned to have highly directional antennas which can be steered towards the angle with maximum power. Hence models for the maximum power are also valuable. Given the custom-designed antenna array at the receiver, our channel sounder is capable of resolving the received power into three-dimensional angles-of-arrival. Accordingly, we provide two pathloss models: one for the maximum-power path and one for the paths combined from all directions.

The paper is organized as follows: Section II describes the channel sounder used to collect measurements and how the measurements were processed into pathloss data points. Section III presents the general breakpoint model we adopted and how its parameters were fit to the model in the environments; discussion on the parameters is provided in this section as well. The paper is concluded with a summary.

II. Measurement System

This section describes the channel sounder we designed and how it measures channel impulse responses (CIRs). Also described is how the responses were processed for the purpose of fitting pathloss models to the data collected.

A. Channel Sounder

The channel sounder consists of a transmitter (TX) section and a receiver (RX) section. At the TX, an arbitrary waveform generator synthesizes a 2047-bit length pseudorandom-noise (PN) code which is BPSK modulated by a 3 GHz intermediate-frequency (IF) carrier. The bit rate of the code is 1 Gbit/s and it occupies a 2 GHz null-to-null bandwidth. The code is repeated continuously. The signal is upconverted to a center frequency of 83.5 GHz and into the transmitter port with 12 dBm power. The antenna is omndirectional in azimuth with a 45° beamwidth in elevation; its gain is 4 dBi.

The front end of the receiver is a custom-designed octagonal waveguide antenna multiplexer (see Figure 1). Connected to the 16 input ports of the array are scalar-feed-horn antennas. The antennas have a 45° beamwidth with an associated gain of 12.2 dBi. Eight of the antennas are oriented toward the horizon while the other eight are oriented 45° upward. This arrangement was chosen to enable coverage of the upper hemisphere. Switching between the output ports is accomplished through sequential on/off biasing of the low-noise amplifiers (LNAs). The LNAs have a 25 dB gain and a noise figure of 6 dB. Together with the other elements of the link budget, the maximum-measureable dynamic range of the system [14] is 140.2 dB. The 16 LNAs are multiplexed into a single waveguide output port. The 83.5 GHz wideband modulated signal from the RX antenna array is then downconverted to a 5 GHz IF and digitized at a rate of 40 Gsymbols/s. Because there are 16 ports and each port is sampled for the duration of two codewords, a complete array sweep lasts 32 codewords or 65.5 µs.

To analyze the measured data, position, velocity, and heading of the receiver array are needed. This information is provided through a robotic mobile positioning system (red box-like apparatus in the foreground of Figure 3(a)). The survey area is first mapped through the robot's laser range-finder. Once the map is created, the onboard computer can direct the robot to waypoints while simultaneously recording position information from the navigation system and controlling the digitizer. In this way, the information can be queried and stored with the digitizer data at millisecond intervals while the robot is moving. Internal studies at NIST have shown position errors of 20 cm at 100 m range and angular errors of ~1°. Further details of the channel sounder and mobile positioning system are provided in [15].

B. Measured Data Points

The system collected measurements at a number of TX-RX configurations throughout each environment. Let i denote the configuration index and d_i the associated distance recorded. At the receiver, the digitized IF signal at the array port was converted to baseband and subsequently correlated with the PN code. This resulted in the impulse response of the channel between the TX and the RX port. A post-distortion filter was applied to remove the system effects through a back-to-back calibration step [16]. That way the output of the filter represented the response of the channel plus the antennas only.

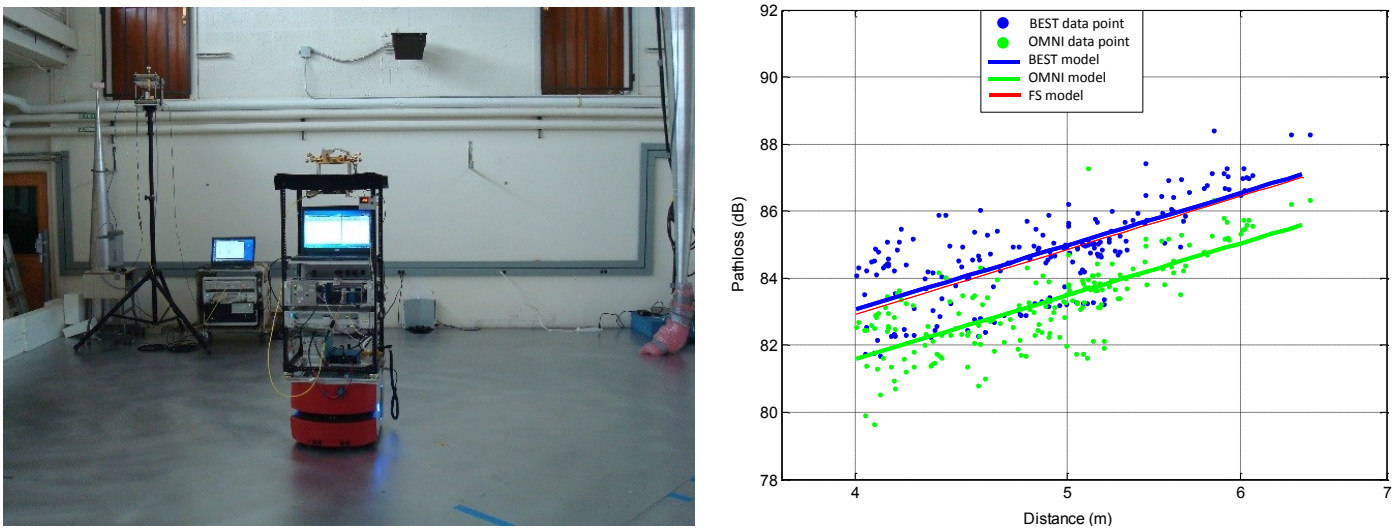

(a) Photograph (b) Pathloss model

Figure 3: Basement environment

The 16 CIRs from one measurement were synthesized through the Space-Alternating Generalized Expectation-maximization (SAGE) algorithm [17] to yield the directional impulse response of the channel. The scope of the algorithm is twofold: 1. to deconvolve the receiver array antenna patterns from the impulse responses; 2. to extract the jth multipath component of the directional channel, namely its complex amplitude (a_{ij}), delay, and angle-of-arrival (azimuth and elevation). Figure 2 displays a three-dimensional plot of the multipath components (elevation dimension is omitted) for an example directional impulse response.

From the extracted multipath components, two pathloss metrics were computed: one for the maximum-power path, PL^{BEST}, and one for the paths combined from all directions, PL^{OMNI}:

$$PL^{BEST}(d_i) = -10\, log_{10} \max_j |a_{ij}|^2 \tag{1a}$$

$$PL^{OMNI}(d_i) = -10\, log_{10} \sum_j |a_{ij}|^2 \,. \tag{1b}$$

For each configuration, 32 measurements were collected over a period of 67 ms while the robot was in motion. Depending on its speed, the robot traveled 20 – 40 mm, roughly seven to ten wavelengths. To factor out small-scale fading, the metrics were averaged over the 32 points. Once collected, the robot downloaded the data and then began measuring for the next configuration. The average distance between configurations was about 30 cm.

III. Pathloss Models

In this section, we present pathloss models for the two environments investigated. The generalized breakpoint model we adopt in decibels is

$$PL(d) = \begin{cases} 10\, \alpha_0\, log_{10}\left(\frac{d}{d_0}\right) + \beta_0 + \mathcal{N}(0, \sigma_0),\ d \le d_1 & \text{(2a)} \\ \overline{PL}(d_1) + 10\, \alpha_1\, log_{10}\left(\frac{d}{d_1}\right) + \beta_1 + \mathcal{N}(0, \sigma_1), d > d_1 & \text{(2b)} \end{cases}.$$

The parameter β_0 denotes the reference pathloss at d_0 = 1 m while α_0 and σ_0 respectively denote the pathloss exponent and standard deviation of the normally distributed shadowing component before the breakpoint distance, d_1. The parameters have analogous values $(\alpha_1, \beta_1, \sigma_1)$ in the second piecewise segment, except for β_1 which is the additional loss above the breakpoint average. The average breakpoint loss is defined as

$$\overline{PL}(d_1) = 10\, \alpha_0\, log_{10}\left(\frac{d_1}{d_0}\right) + \beta_0. \tag{3}$$

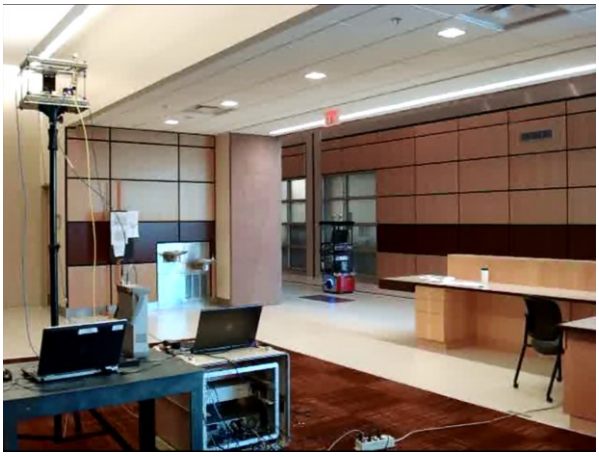

(a) Photograph

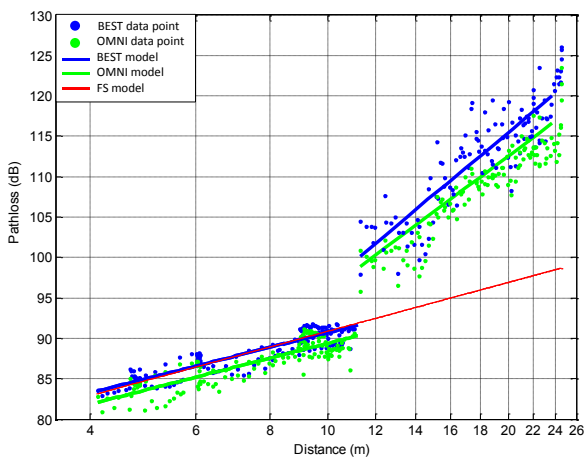

(c) Pathloss models for TX3

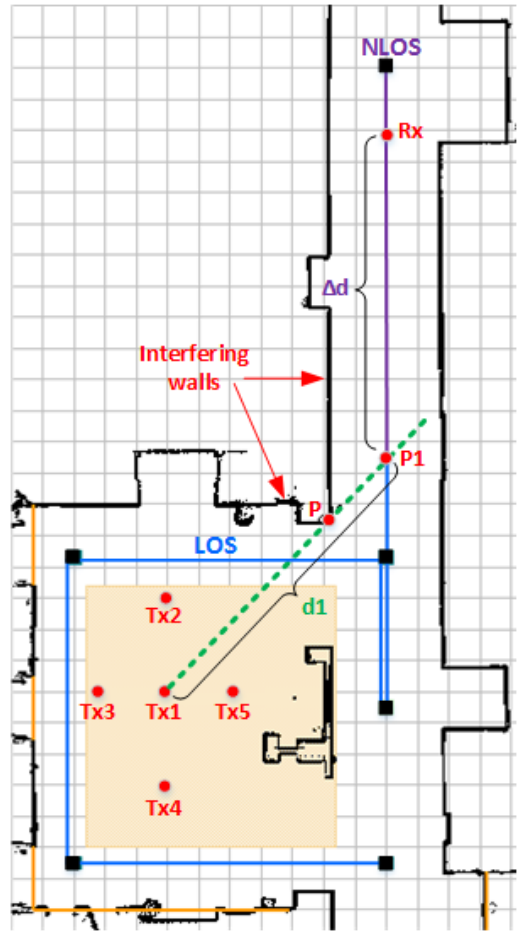

(b) Floorplan

Figure 4. The Lobby / Hallway environment

A. Basement Environment

The first indoor environment we considered is the basement[1] area shown in Figure 3(a). The floor of this area is a metal ground plane and the walls of the room are cinderblock. The room ceiling is 4.9 m high. The photograph shows a hotspot set-up, which applies to all environments described in this paper, with the transmitter antenna fixed at 2.5 m height (background left, mounted on the tripod) and the receiver antenna at 1.6 m (foreground middle, mounted on the robot).

Figure 3(b) illustrates the BEST pathloss model for the Basement as a blue line. It was obtained by fitting (2a) to the $PL^{BEST}(d_i)$ data (blue dots) in (1a) through least-squares regression. Because all measurements were in LOS and the range was so small (less than 7 m), no breakpoint was necessary. Also shown in the plot is the free-space (FS) model [18] in red. The fit to the FS is good, both in terms of $\alpha_0^{BEST} = 1.97$ ($\alpha^{FS} = 2.0$) and $\beta_0^{BEST} = 71.17$ dB ($\beta^{FS} = 70.85$ dB). The nominal transmitter / receiver antenna patterns from the manufacturer were used in the SAGE algorithm (Section II.B) since the antennas have not yet been properly calibrated in an anechoic chamber. The maximum variation from spec is listed as 2 dB to which we attribute deviations of the data points from the FS line.

The OMNI pathloss model (green line) was similarly obtained from the $PL^{OMNI}(d_i)$ data (green dots) in (1b) instead. Notice that the difference between BEST and OMNI is about 1.4 dB; this means that the maximum path accounts for 72% of the total power and conversely that the secondary paths account

[1] The area is actually a laboratory, but since the walls are cinderblock and there are no windows, it is representative of a basement.

environment	# data points	range (m)	wall materials	α_0	β_0 (dB)	σ_0 (dB)	d_1 (m)	α_1	β_1 (dB)	σ_1 (dB)
Basement	351	4.0 – 6.5	cinderblock	1.97	71.18	1.09				
				1.96	69.80	0.86				
Lobby / Hallway TX1	234	4.0 – 21.4	stone / wood / metal	2.37	67.87	2.34	10.1	7.45	2.66	3.87
				2.39	66.85	1.73		5.30	3.94	2.28
Lobby / Hallway TX2	210	4.0 – 18.5		1.75	73.26	1.13	7.8	4.21	14.92	3.74
				1.46	74.66	1.22		3.00	12.96	1.92
Lobby / Hallway TX3	296	4.1 – 22.0		1.87	72.00	1.25	11.3	6.16	8.44	3.04
				1.90	70.41	1.41		5.52	7.09	2.03
Lobby / Hallway TX4	241	4.0 – 24.0		2.05	70.16	1.27	13.3	4.38	4.40	5.35
				2.05	69.34	1.10		4.11	3.48	3.83
Lobby / Hallway TX5	217	5.0 – 20.6		1.57	74.49	1.19	9.6	3.35	6.10	5.08
				1.68	72.70	1.19		3.00	5.38	3.73

Table 1: Environment settings and pathloss model parameters. The light- and dark-shaded entries pertain respectively to the BEST and OMNI models only.

for only 28% of it. Furthermore, because each data point in OMNI also incorporates many other secondary arrivals, the fluctuation in the max arrival will be dampened by the fluctuations in the other arrivals. For this reason, OMNI exhibits a smaller standard deviation (σ_0^{OMNI} = 0.86 dB) compared to BEST (σ_0^{BEST} = 1.09 dB) in this environment and, as we shall see, in the other environment for the most part. Table I shows the settings and pathloss model parameters for the environments.

B. Lobby / Hallway Environment

In the second environment that we investigated, the transmitter was placed at five different locations in a lobby area connected to a hallway. The ceiling heights of the lobby and hallway are 3 m and 7 m respectively. A photograph of the environment is pictured in Figure 4(a) and the locations (TX1 – TX5) are shown on the floorplan in Figure 4(b). For each location, the robot traversed the same trajectory delineated by the black waypoints: the LOS segment appears in blue and the NLOS in purple. Non-line-of-sight was created by the interfering walls when the direct path was lost at breakpoint P_1 as the RX moved down the hallway. The breakpoint was computed analytically as the intersection of the line (green dotted) containing the TX position and the corner (P) and the line along the robot's trajectory in the hallway. The breakpoint distance, d_1, is given as the distance from the TX to this point. Note that each transmitter has a distinct breakpoint.

The breakpoint served to partition the collected pathloss data into LOS and NLOS points. First, for each TX, the $(\alpha_0, \beta_0, \sigma_0)$ parameters were extracted from the LOS points and used to compute $\overline{PL}(d_1)$ from (3). The latter was then subtracted from the measured pathloss of the NLOS points. Finally, rearranging (2b), the parameters $(\alpha_1, \beta_1, \sigma_1)$ were fit to the difference:

$$PL(d) - \overline{PL}(d_1) = 10\,\alpha_1\, log_{10}\left(\frac{d}{d_1}\right) + \beta_1 + \mathcal{N}(0, \sigma_1). \quad (4)$$

For $d > d_1$, the distance was computed as $d = d_1 + \Delta d$, where Δd denotes the incremental distance along the hallway (see Figure 4(b)). This metric provided a better fit than the Euclidean distance and is supported by evidence in [19][20]. The better fit stems from the fact that at this center frequency there is no noticeable wall penetration by the signal; it is therefore more accurate to model the distance along the maximum propagation path.

Table I shows the parameter values for the five TX locations. For instance, consider the pathloss model for TX3 in Figure 4(c). In line-of-sight conditions, the extracted parameters match well to freespace, as before, and the difference between BEST and OMNI is about 1.6 dB (secondary power accounts for 31% of total power), comparable to Basement. In non-line-of-sight, the direct path is lost and so the propagation mechanisms of the dominant path (diffraction and reflection rather than direct transmission) are the same as the secondary paths. This is why the exponent and the standard deviation both increase precipitously from α_0^{BEST} = 1.87 to α_1^{BEST} = 6.16 and from σ_0^{BEST} = 1.25 dB to σ_1^{BEST} = 3.04 dB respectively. Although they experience the same propagation mechanisms, the exponent of OMNI is smaller than BEST, meaning that the dominant path dies down at a faster rate than the secondary paths. From the different exponents, it follows that the gap between BEST and OMNI begins to widen at the breakpoint and ultimately reaches 3.4 dB. At this end range, the secondary power accounts for more than half of the total power.

IV. Summary and Conclusion

In this paper, we presented pathloss models for indoor hotspot deployment at 83.5 GHz. The indoor environments investigated are typical of such deployments, namely a basement, lobby, and hallway in line- and non-line-of-sight conditions up to a range of 24 m. To fit the models, a custom-designed channel sounder recorded measurements over 1500 different transmitter-receiver configurations. In LOS, a good match was observed between our pathloss models and freespace prediction, validating our calibration procedures. In NLOS, the pathloss exponents increased precipitously, varying between 3.00 and 7.45 depending on the model and the TX position. This is because the direct path goes undetected due to the high penetration loss of the interfering walls at this frequency.

References

[1] "Cisco Visual Networking Index: Global Mobile Data Traffic Forecast Update, 2015–2020," white paper, Feb. 2016.

[2] Federal Communications Commission Office of Engineering and Technology Policy and Rules Divison, "FCC Online Table of Frequency Allocations," 47 C.F.R. § 2.106, March 2016.

[3] T.S. Rappaport, S. Shu, R. Mayzus, H. Zhao, Y. Azar, K. Wang, G.N. Wong, J.K. Schulz, M. Samimi, and F. Gutierrez, "Millimeter wave mobile communications for 5G cellular: It will work!" *IEEE Access*, vol. 1, pp. 335-349, May 2013.

[4] M. Lei, J. Zhang, T. Lei, D. Du, "28-GHz indoor channel measurements and analysis of propagation characteristics," *IEEE Personal, Indoor, and Mobile Radio Communication Conf.*, pp. 208-212, Sept. 2014.

[5] O.H. Koymen, A. Partyka, S. Subramanian, J. Li, "Indoor mm-Wave Channel Measurements: Comparative Study of 2.9 GHz and 29 GHz," *IEEE Global Communications Conf.*, pp. 1-6, Dec. 2015.

[6] N. Moraitis, P. Constantinou, "Indoor channel measurements and characterization at 60 GHz for wireless local area network applications," *IEEE Transactions on Antennas and Propagation*, vol. 52, no. 12, pp. 3180 -3189, Dec. 2004.

[7] S. Geng, J. Kivinen, X. Zhao, P. Vainikainen, "Millimeter-Wave Propagation Channel Characterization for Short-Range Wireless Communications," *IEEE Transactions on Vehicular Technology,* vol. 58, no. 1, pp. 3-13, Jan. 2009.

[8] M.-W. Jung, J. Kim, Y.-K. Yoon, "Measurements of path loss in MM-wave for indoor environments," *IEEE Asia Pacific Microwave Conf.*, pp. 1068-1071, Dec. 2009.

[9] K. Haneda, J. Järveläinen, A. Karttunen, M. Kyrö, and J. Putkonen, "A Statistical Spatio-Temporal Radio Channel Model for Large Indoor Environments at 60 and 70 GHz," IEEE Trans. on Antennas and Propagation, vol. 63, no. 6, pp. 2694-2704, June 2015.

[10] M. Jacob and T. Kurner, "Radio channel characteristics for broadband WLAN/WPAN applications between 67 and 110 GHz," *IEEE European Conf. on Antennas and Propagation*, pp. 2663 - 2667, March 2009.

[11] A. Kajiwara, "Indoor propagation measurements at 94 GHz," *Personal, Indoor, and Mobile Radio Communications Conf*., pp. 1026-1030, Sept. 1995.

[12] J. Helminger, J. Detlefsen, H. Groll, "Propagation properties of an indoor-channel at 94 GHz," *Intl. Conf. on Microwave and Millimeter Wave Technology*, pp 9-14, Aug. 1998.

[13] S. Deng, M.K. Samimi, T.S. Rappaport, "28 GHz and 73 GHz Millimeter-Wave Indoor Propagation Measurements and Path Loss Models," IEEE Intl. Conf. on Communications, pp. 1244-1250, June 2015.

[14] T.S. Rappaport, G.R. MacCartney, Jr., M.K. Samimi, and S. Sun, "Wideband Millimeter-Wave Propagation Measurements and Channel Models for Future Wireless Communication System Design," IEEE Trans. on Communication, vol. 63, no. 9, pp. 3029-3056, Sept. 2015.

[15] P.B. Papazian, C. Gentile, K.A. Remley, J. Senic, and N. Golmie, "A Radio Channel Sounder for Mobile Millimeter-Wave Communications: System Implementation and Measurement Assessment," *To appear in IEEE Transactions on Microwave Theory and Techniques*, Jan. 2017.

[16] P.B. Papazian, J.-K. Choi, J. Senic, P. Jeavons, C. Gentile, N. Golmie, R. Sun, D. Novotny, K.A. Remley, "Calibration of Millimeter-wave Channel Sounders for Super-resolution Multipath Component Extraction," *IEEE European Conf. on Antennas and Propagation*, pp. 1-5, April 2016.

[17] K. Hausmair, K. Witrisal, P. Meissner, C. Steiner, G. Kail, "SAGE Algorithm for UWB Channel Parameter Estimation," *COST 2100 Management Committee Meeting*, pp. 1-7. Feb. 2010.

[18] H. Friis, "A note on a simple transmission formula,*" Proceedings of the IRE*, vol. 34, no. 5, pp. 254–256, May 1964.

[19] D.W. Matolak, K.A. Remley, C. Gentile, C.L. Holloway, Q. Wu, and Q. Zhang, "Peer-to-Peer Urban Channel Characteristics for Two Public-Safety Frequency Bands," *IEEE Antennas and Propagation Magazine*, vol. 56, no. 5, pp. 101-115. Oct. 2014.

[20] A.F. Molisch, A. Karttunen, S. Hur, J. Park, J. Zhang, "Spatially consistent pathloss modeling for millimeter-wave channels in urban environments," *IEEE European Conf. on Antennas and Propagation*, pp. 1-5, April 2016.